ASSIMILATIVE FORECASTING OF THE ENERGETIC PARTICLE ENVIRONMENT

S. Naehr
Department of Physics and Astronomy
Rice University
6100 Main Street, Mail Stop 108
Houston, TX 77005
Phone: (713) 348-2408
E-mail: naehr@rice.edu

F. Toffoletto
Rice University

Abstract

We present a computational approach to specifying and forecasting the outer radiation belt particle distribution, by incorporating data from space-based measurements. In this approach, a Kalman-Bucy filter is designed to assimilate particle flux data from a spacecraft spanning a broad range of particle drift paths. A spatial analysis algorithm is used to incorporate this data into the framework of a physics-based forecast model, using the statistical error structures of the model and data to produce an optimal estimate. The assimilation algorithm is validated in a set of experiments simulating a magnetic storm, using artificial magnetic field and particle flux data fabricated by an independent model. The simulated data is compared to the model over the entire modeling region at each time step, providing a global assessment of the model's accuracy over the course of dynamically active period.

Introduction

Our ability to forecast the environment of energetic particles trapped within the Earth's magnetosphere is limited by our incomplete understanding of the physical processes involved, and by our inability to accurately represent the dynamic behavior of the magnetic field. This paper describes an approach to overcoming these limitations, by incorporating real-time *in situ* data into a physics-based dynamic model. Techniques in spatial analysis and data assimilation, widely used in atmospheric weather modeling, are adapted to the problem of modeling the trapped radiation environment with a limited number of space-based observations.

The greatest difficulty in applying these techniques to the modeling of magnetospheric phenomena is the sparseness of real-time data. In the case of the radiation belts, for example, there are seldom more than two or three satellites providing simultaneous measurements of particle flux at points throughout the magnetosphere, and these measurements tend to be largely concentrated in geosynchronous orbit. However this situation is likely to change in the near future, as the number of spacecraft put into orbit for scientific, military, and commercial purposes continues to increase.

In anticipation of increasing data availability, we have begun to develop the theory and computational tools needed to incorporate data into a variety of magnetospheric models, such as

the radiation belt model described in this paper. While the full benefits of this approach may not become clear until the observing system becomes more complete, the results presented below suggest that the assimilation of even a few observations may significantly improved the accuracy of specification and forecast models.

The next section provides a brief overview of the data assimilation techniques employed in this study, with emphasis on the terminology and mathematical formalism guiding our approach. Section 3 describes the application of this formalism to a simple model of radiation belt particle dynamics. In section 4, we describe a simulated magnetic storm scenario that is used to test the data assimilation algorithm. The results of these tests are presented in section 5, and in section 6 we assess the viability of our approach and consider its extension to more complicated and realistic situations.

Data Assimilation

The data assimilation approach used in this paper is known as the Kalman-Bucy filter, originally devised for linear systems of ordinary differential equations [*Kalman*, 1960, *Kalman and Bucy*, 1961]. The Kalman-Bucy (KB) filter has two main components: spatial analysis and prediction. The spatial analysis algorithm combines localized observations with a model-computed background configuration to estimate the most probable state of the entire model system at a particular time. The prediction algorithm propagates the configuration forward in time, using the physical rules of the forecast model to govern the evolution of the system. In the KB filter, the output of the prediction algorithm forms the background configuration for subsequent spatial analysis.

In the spatial analysis portion of the KB-filter, observations are incorporated into the background configuration of the system by a process known as statistical interpolation, originally devised by *Kolmogorov* [1941] and *Wiener* [1949]. Statistical interpolation is essentially a weighted least-squares fit between observed and background values, in which the statistical weights are functions of the errors and correlations (known or estimated) associated with each value.

The formalism of statistical interpolation can be defined as follows. Suppose at a time t_n the configuration or state of a system is defined by a set of quantities $\underline{s}_n$, where $\underline{s}_n$ is a vector of length L (hereafter a single underline denotes a column vector, and double underlines a rank-2 array). The state vector might represent, for example, the value of some physical quantity on a regular grid of locations $\mathbf{r}_1, \mathbf{r}_2, \mathsf{K}, \mathbf{r}_L$. An empirical model or a previous forecast provides a background estimate of the state $\underline{s}_n^{\mathrm{F}}$. Further suppose that at t_n there exists K observations $\underline{d}_n$ of a physical quantity d, which is related to the global state $\underline{s}_n$ by

$$d_n = H_n(\underline{s}_n) \qquad (1)$$

For example, d might be the value of s at an observing location $\mathbf{r}_o$, which does not (in general) coincide with a point on the model grid. In this case $H(\underline{s})$ is simply an interpolation of the state variables onto the point $\mathbf{r}_o$. More generally H can be any linear or non-linear transformation or

interpolation of the state vector $\underline{s}_n$. If H is a linear function of the state variables, then it may be written as a $K \times L$ array defined by

$$\underline{d}_n = \underline{\underline{\mathrm{H}}}_n \, \underline{s}_n \qquad (2)$$

The background, observations, and transformation function may all contain errors, and in general these errors may be correlated to one another. The expected covariances among the errors are assumed to be known, unbiased, and normally distributed. They are expressed in the statistical interpolation formalism by *error covariance matrices*. The background error covariance matrix is defined in terms of the errors $\varepsilon_n^F = s_n^F - s_n^{\text{true}}$ at each grid point by

$$\left[\underline{\underline{\mathrm{P}}}_n^F\right]_{ij} = \left\langle \varepsilon_n^F(\mathbf{r}_i)\varepsilon_n^F(\mathbf{r}_j) \right\rangle \qquad (3)$$

where the angle brackets denote the expectation operator. The observation error covariance $\underline{\underline{\mathrm{R}}}_n$ matrix is similarly defined, but includes errors and correlations associated with the function $H(\underline{s})$ as well as the observations themselves.

With these definitions, the statistical interpolation procedure is [*Daley,* 1991]

$$\underline{s}_n^{\mathrm{A}} - \underline{s}_n^{\mathrm{F}} = \underline{\underline{\mathrm{K}}}_n \left[\underline{d}_n - \underline{\underline{\mathrm{H}}}_n \underline{s}_n^{\mathrm{F}}\right] \qquad (4)$$

$$\underline{\underline{\mathrm{K}}}_n = \underline{\underline{\mathrm{P}}}_n^{\mathrm{F}} \underline{\underline{\mathrm{H}}}_n^{\mathbf{T}} \left[\underline{\underline{\mathrm{R}}}_n + \underline{\underline{\mathrm{H}}}_n \underline{\underline{\mathrm{P}}}_n^{\mathrm{F}} \underline{\underline{\mathrm{H}}}_n^{\mathbf{T}}\right]^{\mathbf{1}} \qquad (5)$$

$$\underline{\underline{\mathrm{P}}}_n^{\mathrm{A}} = \left[\underline{\underline{\mathrm{I}}} - \underline{\underline{\mathrm{K}}}_n \underline{\underline{\mathrm{H}}}_n\right] \underline{\underline{\mathrm{P}}}_n^{\mathrm{F}} \qquad (6)$$

The vector $\underline{s}_n^{\mathrm{A}}$ is the analyzed state of the system—that is, the most probable set of values given the background $\underline{s}_n^{\mathrm{F}}$, observations $\underline{d}_n$, and the corresponding error covariance matrices. The matrix $\underline{\underline{\mathrm{K}}}_n$ is a set of weighting coefficients, which essentially determines the statistical significance of each observation in $\underline{d}_{\mathrm{n}}$ to the analysis. The matrix $\underline{\underline{\mathrm{P}}}_n^{\mathrm{A}}$ is the analysis error covariance matrix; it contains the expected errors and correlations associated with $\underline{s}_n^{\mathrm{A}}$.

The prediction part of the KB-filter is defined by the forecast model. In the following we assume that the evolution of the system from time t_{n} to t_{n+1} can be represented by a linear matrix operator $\underline{\underline{\mathrm{M}}}_n$ acting on the state vector at t_n. The forecast is assumed to be imperfect, with a known error covariance matrix $\underline{\underline{\mathrm{Q}}}_n$. Given the analyzed state vector and its error covariance matrix, the forecast state and error covariance matrix are given by

$$\underline{s}_{n+1}^{\mathrm{F}} = \underline{\underline{\mathrm{M}}}_n \underline{s}_n^{\mathrm{A}} \qquad (7)$$

$$\underline{\underline{\mathrm{P}}}_{n+1}^{\mathrm{F}} = \underline{\underline{\mathrm{M}}}_n \underline{\underline{\mathrm{P}}}_n^{\mathrm{A}} \underline{\underline{\mathrm{M}}}_n^{\mathbf{T}} + \underline{\underline{\mathrm{Q}}}_n \qquad (8)$$

Equations (4)-(8) provide the governing equations of the data assimilation algorithm in a general form. The next section describes the application of this algorithm to the specific problem of modeling radiation belt dynamics.

Model

The Kalman-Bucy filter can be applied to a variety of dynamic systems. In this section we describe the application of a KB-filter to a simple model of radiation belt dynamics. The physical basis of the forecast model is briefly outlined, and cast into a computational form consistent with the KB-filter equations (4)-(8). We next discuss the transformation/interpolation of observed fluxes onto the model grid, using an estimate of the magnetic field configuration computed by an independent model.

Forecast model

The forecast model used in this study considers the phase space density of relativistic (MeV-range) electrons stably trapped in the radiation belts. For these particles we assume that the adiabatic invariants J_1, J_2, J_3 associated with the particle gyration, bounce, and drift motions are approximately conserved, except for small stochastic fluctuations. Under this assumption the evolution of the particle distribution can be represented by diffusion in the adiabatic invariants, of the form

$$\frac{\partial f(J_1,J_2,J_3;t)}{\partial t} = \sum_i \sum_j \frac{\partial}{\partial J_i}\left[D_{ij} \frac{\partial f(J_1,J_2,J_3;t)}{\partial J_j} \right] \quad (9)$$

Here D_{ij} are diffusion coefficients, related to the expected rate of change in each adiabatic invariant. For simplicity we limit our investigation to equatorially mirroring particles—that is, particles with zero second adiabatic invariant, in a magnetic field configuration where the minimum field strength along each field line lies in the equatorial plane. Such particles are entirely confined to the equatorial plane, and drift along paths of constant field strength. We further assume that diffusion in the first adiabatic invariant and losses (due to collisions with the Earth's atmosphere, e.g.) are negligible, so that the governing equation becomes a simple 1D diffusion equation in the third adiabatic invariant. Using μ for the first adiabatic invariant and the Roederer L parameter $L \propto J_3^{-1}$ in place of the third, the radial diffusion equation is

$$\frac{\partial f(\mu,L,t)}{\partial t} = L^2 \frac{\partial}{\partial L}\left[\frac{D_{LL}}{L^2} \frac{\partial f(\mu,L,t)}{\partial L} \right] \quad (10)$$

We assume a time-independent diffusion coefficient of the form

$$D_{LL} = D_0 L^n \quad (11)$$

with quiet-time values $D_0 = 7.905 \times 10^{-12}$ hrs^{-1} and $n = 11.7$ adopted from the study of *Selesnick et al.* [1997].

Computationally, the diffusion equation is solved in discretized form by the Crank-Nicholson numerical method – a semi-implicit approach with second-order accuracy in both space and time. For the interior grid points (l = 2, 3, … , N-1), the distribution at $t = t_{n+1}$ is defined by

$$\left[-\alpha(1-\beta)\right]f_{l-1}^{n+1} + (1+2\alpha)f_l^{n+1} + \left[-\alpha(1+\beta)\right]f_{l+1}^{n+1} = \alpha(1-\beta)f_{l-1}^{n} + (1-2\alpha)f_l^{n} + \alpha(1+\beta)f_{l+1}^{n} \quad (12)$$

$$\alpha = \frac{1}{2}\frac{D_0 L^n \Delta t}{(\Delta L)^2}, \quad \beta = \frac{(n-2)\Delta L}{2L} \quad (13)$$

The end-point values are determined by the boundary conditions. At the inner boundary of the modeling region where $L \sim 1$, the diffusion coefficient D_{LL} becomes vanishingly small; hence f is very nearly constant at the inner boundary, so $f_{l=1}^{n+1} = f_{l=1}^{n}$. Since the outer boundary distribution is unknown (unless an observation happens to be available), a Neumann-type (zero slope in f) outer boundary condition is applied at $l = N$. To second order accuracy in space, the discrete outer boundary condition is thus

$$3f_N^{n+1} - 4f_{N-1}^{n+1} + f_{N-2}^{n+1} = 0 \quad (14)$$

The discretized governing equations and boundary conditions can be conveniently summarized in matrix form. Writing the set of value $[f_l^n, l = 1,2, \ldots]$ as the column vector $\underline{s}_n$, we have

$$\underline{\underline{A}}\,\underline{s}_{n+1} = \underline{\underline{B}}\,\underline{s}_n \quad (15)$$

or, equivalently,

$$\begin{aligned} \underline{s}_{n+1} &= \underline{\underline{M}}\,\underline{s}_n \\ \underline{\underline{M}} &= \underline{\underline{A}}^{-1}\underline{\underline{B}} \end{aligned} \quad (16)$$

The square matrices $\underline{A}$ and $\underline{B}$ are nearly tridiagonal, with interior elements defined by equation (12), and first and last rows defined by the boundary conditions.

The set of phase space densities f, defined on a grid of discrete values of μ and L, represents the state-vector characterizing the configuration of the system. The discretized radial diffusion operator and boundary conditions of equations (12)-(16) form the forecast matrix $\underline{M}_n$ in equation (7). This matrix completely describes the evolution of the phase space density distribution over time, given an initial state.

The KB-filter additionally requires an initial estimate of the state at $t_{n=0}$, and error covariance matrices associated with both the initial state and the forecast model. In the test simulations described below, the initial distribution function is specified arbitrarily, and the errors associated with it are assumed to be large and uncorrelated. Since the forecast error covariance matrix is continuously modified with each data assimilation cycle (equations (6) and (8)), the algorithm is not especially sensitive to its initial value. The forecast error covariance matrix $\underline{Q}$ is somewhat more complicated: it represents both errors in the discretization of the forecast equation (10), and variations in the true system that are not represented by the forecast equation. These errors of representativeness are difficult to quantify. In the present study we make the simplest possible approximation, in which the expected forecast errors are uncorrelated and equal to a constant.

Spatial analysis

The analysis portion of the KB-filter requires a set of observations $\underline{d}_n$ and a transformation function $H_n(\underline{s}_n)$ for each time t_n For our model system the observations are taken to be measurements of differential directional flux at discrete energy levels, obtained at regular intervals along the orbit of a spacecraft confined to the equatorial plane. The differential directional flux j of particles with momentum p is simply related to the phase space density by

$$j = p^2 f \tag{17}$$

Since the forecast model operates in an adiabatic invariant coordinate system rather than physical space, it is necessary to determine the adiabatic invariants associated with each observation. These quantities depend on the configuration of the magnetospheric magnetic field. For a given observation position **r** and kinetic energy E (or corresponding momentum p), they are given by

$$\mu = \frac{p^2}{2mB(\mathbf{r})} \tag{18}$$

$$L = 2\pi B_0 R_E^2 \Phi^{-1}, \quad \text{where} \quad \Phi = \oint\!\!\oint_{\text{drift path}} B(\mathbf{r})\, \mathrm{d}A \tag{19}$$

The magnetic field configuration must be supplied by another model, and is considered an input to the assimilation model. In principle, any magnetic field model, whether empirical, theoretical, or even a simple dipole field, can be used. However the likely error (and error correlations) associated with the model must be estimable, as these are also input to the spatial analysis algorithm. In this study we presuppose a magnetic field model that provides the magnetic field strength B, the L parameter, and the associated error covariances for any input set of positions **r** in the equatorial plane

Given estimates of μ and L corresponding to the observation, the function H becomes a two-dimensional interpolation onto the model grid. For simplicity we use a bilinear interpolation of the form

$$H_{ml}(\mathbf{r}, E) = p(E)^2 c_m(\mathbf{r}, E) d_l(\mathbf{r}) \tag{20}$$

The coefficients c and d are given by

$$c_m(\mathbf{r}, E) = \begin{cases} \frac{\mu_{m+1} - \mu(\mathbf{r},E)}{\mu_{m+1} - \mu_m}, \mu_m \le \mu(\mathbf{r},E) < \mu_{m+1} \\ \frac{\mu(\mathbf{r},E) - \mu_{m-1}}{\mu_m - \mu_{m-1}}, \mu_{m-1} \le \mu(\mathbf{r},E) < \mu_m \\ 0 \quad , \text{all other } m \end{cases} \qquad d_l(\mathbf{r}) = \begin{cases} \frac{L(\mathbf{r}) - L_l}{L_{l+1} - L_l} \quad , L_l \le L(\mathbf{r}) < L_{l+1} \\ \frac{L_{l-1} - L(\mathbf{r})}{L_l - L_l - 1}, L_{l-1} \le L(\mathbf{r}) < L_l \\ 0 \quad , \text{all other } l \end{cases} \tag{21}$$

The final element needed for the KB-filter is the observation error covariance matrix. This matrix has two components: covariances associated with the instrument error of the observing

satellite, and error covariances produced by the transformation function H. In the following we assume that instrument errors are known and uncorrelated. The errors associated with the transformation function are assumed to be dominated by errors in the values of μ and L computed by the magnetic field model. The error ε_H in H is related to the errors ε_μ and ε_L to first order by

$$\varepsilon_H(\mathbf{r},E) \approx p(E)^2 \left[\left. \frac{\partial f}{\partial \mu} \right|_{\mu(\mathbf{r},E)} \varepsilon_\mu(\mathbf{r},E) + \left. \frac{\partial f}{\partial L} \right|_{L(\mathbf{r})} \varepsilon_L(\mathbf{r}) \right] \tag{22}$$

The observation error covariance matrix is then constructed from the covariances among the ε_H for each energy channel and position of the observation set, together with the expected error variance of the observed fluxes.

Simulated Storm

In order to test the data assimilation algorithm, a simple scenario was constructed, in which a storm-time enhancement of the outer radiation belts is observed by a single spacecraft traversing the radiation belts. While not necessarily realistic, the use of fabricated data in this testing procedure allows us to control and simplify the behavior of the system, to more easily identify the response of the assimilation algorithm to various factors. Furthermore the simulated system provides a global picture of the "true" evolution of the system, against which the assimilation algorithm can easily be compared.

The observing system in this simulation is a single satellite measuring differential directional flux in ten channels of kinetic energy E = 1, 2, 3, …, 10 MeV. The satellite lies in the equatorial plane, on an elliptical orbit with 24-hour period. The satellite's orbit crosses a wide range of L shells, from $L \sim 1.2$ to beyond the outer modeling boundary L = 10, as shown in figure 1. Satellite measurements are computed and delivered to the assimilation algorithm once per hour; measurements beyond the modeling boundary are simply ignored. The fluxes measured by the satellite are computed from the true phase space density distribution and magnetic field configuration described below.

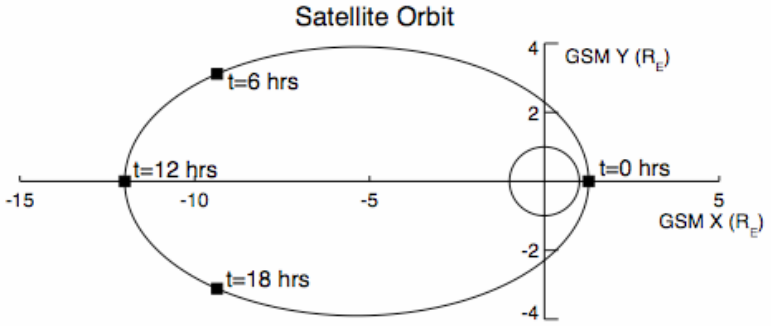

Figure 3. Orbital path (in magnetic equatorial plane) of satellite providing data during the simulated storm. Black squares indicate the spacecraft's position at 6, 12, and 18 hours from perigee. The orbital period is 24 hours.

The simulated environment consists of a simple magnetic field model, and a time-dependent phase space density distribution. The initial phase space density was chosen to be constant in L, with a simple power-law dependence in μ given by $f \propto \mu^{-5}$. The magnetic field model consists of the Earth's dipole field B_D (with zero tilt) and a time-dependent symmetric ring current B_{RC}, parameterized by the field depression Dst at the equator:

$$B(r,t) = B_D(r) + Dst(t)\, B_{RC}(r) \qquad (23)$$

$$B_D = \frac{B_0 R_E^3}{r^3}, \quad B_{RC} = \frac{r - r_0}{1 - r_0} \qquad (24)$$

Over the course of the 10-day simulation period, the system underwent a "storm" in which the ring current became stronger, and phase space densities at the outer boundary of the modeling region at $L = 10$ were enhanced by an order of magnitude for all values of μ. The time variation of the ring current parameter and outer boundary condition over the course of the simulation are shown in figure 2.

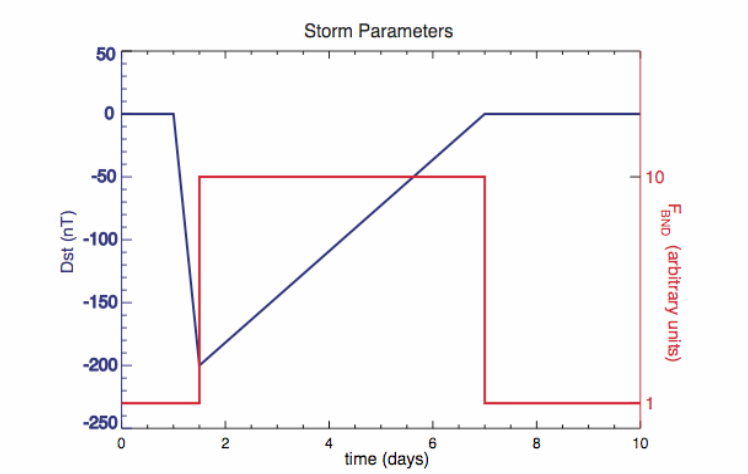

Figure 2. Time-variation of the simulated storm parameters Dst and F_{BND}, as described in the text.

The enhancement of phase space density at $L = 10$ was propagated inward to low L by the radial diffusion defined in equations (10) and (11), with Dirichlet rather than Neumann outer boundary conditions. Figure 3 depicts the evolution of the phase space density at μ = 5623 MeV/G as a function of L and time over the course of the simulation. In this simulation the evolution at other values of μ is identical.

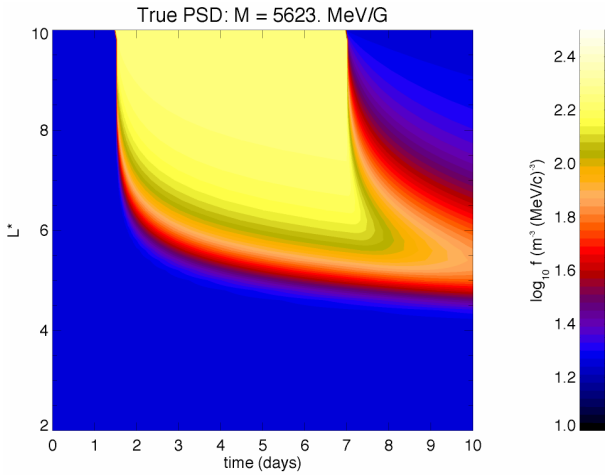

Figure 3. Contours of phase space density at μ = 5623 MeV/G vs. *L* and time, for the true (simulated) electron population.

Results

The data assimilation algorithm described in sections 2 and 3 was used to model the response of the radiation belt electrons to the simulated storm described above. The correct initial distribution at the beginning of the event was supplied to the assimilation model, in order to better illustrate the model's ability to capture dynamic changes to the system.

The model computes changes in phase space density at each time step by solving the radial diffusion equation with Neumann boundary conditions. Since the initial distribution is constant in *L* and therefore a steady state solution to equation (10), the forecast model predicts absolutely no change in the phase space density over the course of the simulation, in the absence of assimilated data.

We first consider an idealized case in which perfect data is supplied to the assimilation algorithm. That is, the fluxes measured by the satellite each hour correspond exactly to the correct phase space density distribution, and the magnetic field model provides a perfect transformation from spatial to adiabatic invariant coordinates. In this case the observation error covariance matrix $\underline{\underline{R}}_n$ in equation (5) is a null matrix. The assimilation model is not without error, however, because the satellite provides the correct phase space density only for a few values of μ at a single value of *L* at each time step. The spatial analysis must spread these discrete points of data over the entire (μ,*L*) grid, and it does so with errors given by equation (6).

Figure 4 shows the predicted phase space density at μ = 5623 MeV/G over the course of the storm, in the same format as that of figure 3. At this value of μ the assimilation does an admirable job of reproducing the correct behavior of the system. The discontinuous changes in *f* that appear periodically reflect the assimilation of new measurements from the satellite. The cadence is approximately 12 hours because the value of μ corresponding to a given energy channel depends strongly on the magnetic field strength, and therefore on the position of the satellite. Thus the phase space density at μ = 5623 MeV/G, which corresponds to ~ 2 MeV at *L* ~ 6.6, is sampled by the satellite in tightly clustered groups around *L* ~ 5-7 on each inbound and

outbound pass. Results similar to those in figure 4 are obtained over a wide range of μ, from ~ 10^3 to 10^5 MeV/G.

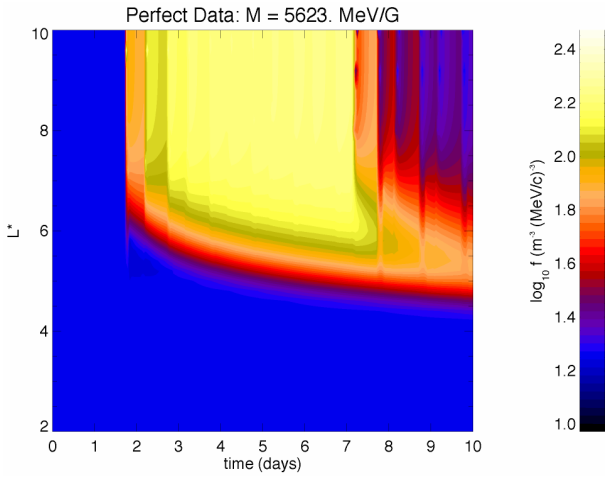

Figure 4. Assimilation model results with perfect observations, in the same format as figure 2.

The spatial analysis algorithm can be quite effective in inferring the complete distribution in *L* from only a few well-placed measurements. However the success of the assimilation algorithm depends strongly on the location of those measurements. Since the observed μ is largely a function of observing position, the model is much less successful at reproducing the phase space density at extreme μ values. Figure 5*a* shows the predicted phase space density at μ = 177.8 MeV/G (the true distribution is nearly identical to figure 3, with the values corresponding to each color offset). The satellite's 1-10 MeV energy channels sample this low μ only at large values of *B* corresponding to positions Earthward of *L* ~ 3, where the true distribution remains virtually constant over time. The storm-time ring current exacerbates this problem by decreasing the field strength in the inner magnetosphere, pushing the sampling range even closer to the Earth. Thus the assimilation fails to capture most of the dynamic changes to the system. Only late in the event, when the ring current has largely subsided, does the satellite begin to sample this value of μ. A similar behavior is seen at very large μ, as shown in figure 5*b*. The spacecraft samples μ = 10^6 only when *B* is less than ~30 nT. Again the satellite encounters this range of *B* only after the ring current (which increases the field strength in the outer magnetosphere) has subsided.

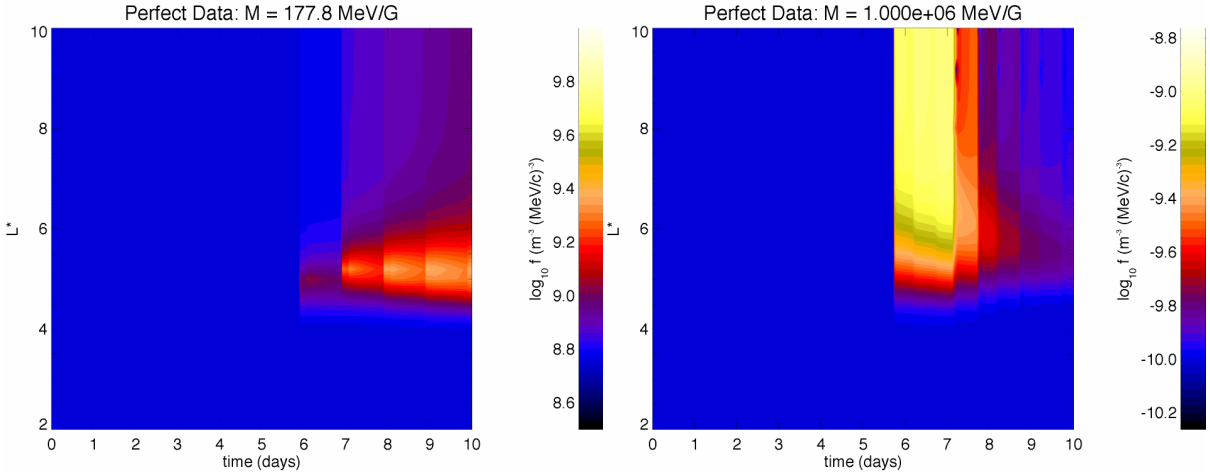

Figure 5. Same as figure 4, at (a) μ = 177.8 MeV/G, and (b) μ = 10^6 MeV/G.

We next consider the effects of various kinds of error on the assimilation results. Figure 6 displays the predicted phase space density at μ = 5623 MeV/G, for an assimilation in which two types of observational error are simulated. The first is an error in the measured flux, simulated by randomly perturbing the correct value. The second is an error in the magnetic field model used to calculate the μ and *L* values corresponding each observation's position and energy channel. The magnetic field errors are generated by randomly perturbing the value of *Dst* in equation (23), and by adding random, spatially uncorrelated field fluctuations with a spatial scale of 1 R_E. The random variations added to the flux, *Dst*, and the perturbation field are all normally distributed, with standard deviations of 10%, 10 nT, and 5 nT, respectively. These expected errors are considered known in the assimilation algorithm, and contribute to the observation error covariance matrix $\underline{\underline{R}}_n$.

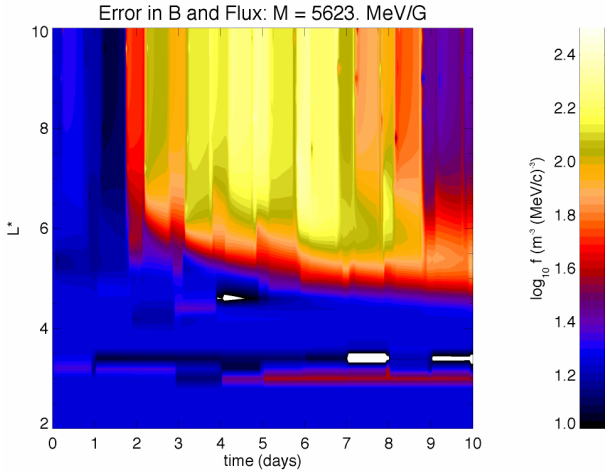

Figure 6. Same as figure 4, with errors in the observed fluxes and magnetic field.

The effect of these errors is evident in the noisy, patchy distribution shown figure 6 (compared to figure 4, for which no errors were included), but the overall picture remains reasonably faithful to the true distribution (figure 3). Errors at low *L* are especially noticeable for two reasons. First, the magnetic field strength is large at low *L*, so only measurements in the

highest energy channels sample μ = 5623 MeV/G. Thus there are fewer total observations at low *L*. Second, diffusion is very slow in this region, so errors introduced at a particular (μ, *L*) tend to persist until repeated measurements at the same values become available. Random fluctuations in the magnetic field make repeated sampling of the same (μ, *L*) an unlikely event.

In figure 7, the effects of errors in the forecast model are shown. Here there are no errors associated with the observations or the magnetic field, but the diffusion coefficient defined by equation (11) is made to be artificially large, scaling as L^{13} rather than $L^{11.7}$. In this model the diffusion coefficient is not modified in the data assimilation cycle, so the forecast consistently overestimates the rate at which enhancements in the phase space density propagate to lower *L*. The observations, however, continually correct this error, creating a sawtooth pattern in the evolution of the enhancement's leading edge over time. The resulting distribution is still reasonable, but by the end of the simulation the enhancement has moved too far Earthward by a margin $\Delta L \sim 1.0$.

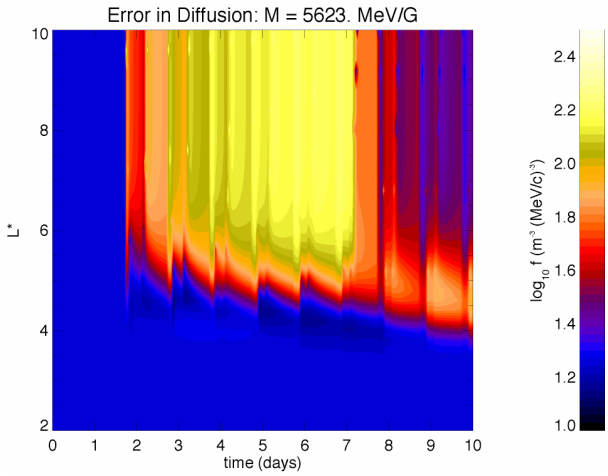

Figure 7. Assimilation results at μ = 5623 MeV/G, with errors in the forecast model diffusion coefficient.

Conclusions

This paper illustrates the application of data assimilation techniques —specifically the Kalman-Bucy filter—to a physics-based model of radiation belt dynamics. A rudimentary assimilation consisting of a single observing spacecraft and a simple forecast model was compared to the prescribed evolution of the radiation belts during a simulated magnetic storm, with encouraging results. The assimilation of even small amounts of data can markedly improve a forecast model, if the observations are fortuitously placed in regions of high uncertainty. When the physics underlying the forecast model is sufficiently realistic, and the errors well known, the spatial analysis algorithm is able to infer the global distribution of the phase space density from these sparse observations with remarkable accuracy. The assimilation model is fairly robust, in that random errors in the observations, magnetic field model, and/or forecast models do not drastically degrade the predicted distribution —provided that the expected errors are accurately represented in the KB-filter formalism.

The development of a realistic radiation belt forecast model will require further research on a number of different fronts. First, the 1D forecast model described above is far too simplistic. It neglects much of the known physics governing the radiation belts, such as losses due to pitch-angle scattering into the loss cone, acceleration mechanisms such as ULF-drift resonance, and variations in the radial diffusion coefficient with time and μ. The application of the KB-filter to a more realistic dynamic model will require careful assessment of the errors and correlations associated with each facet of the model.

A realistic assimilation model will also require a far more sophisticated representation of the magnetic field. The one-parameter, azimuthally symmetric field model used above is clearly a poor representation of the magnetosphere. Fortunately there already exist advanced, data-based models of the magnetospheric magnetic field (e.g., *Tsyganenko*, 2002), which can be readily adapted to the assimilation model described here. However, as with the forecast model, the errors and correlations associated with the selected magnetic field model must be reliably estimated.

Finally, the assimilation model must be tested will actual data. This will require realistic estimation of the instrument error and background noise level associated with each measurement, and a careful selection of events based on data availability. In particular, the assimilation must be tested on events in which at least two independent sets of observations are available, so that the accuracy of the model can be assessed.

The work presented here represents a preliminary step toward assimilative modeling of the radiation belts. While the development of a fully realistic assimilation model faces a considerable number of challenges, the results presented here demonstrate the potential of the assimilation techniques employed here to significantly improve the specification and forecasting capabilities of dynamic models.

References

1. Daley, R., Atmospheric data analysis, Cambridge University Press, New York, 1991.

2. Kolmogorov, A., Interpolated and extrapolated stationary random sequences, Isvestia an SSSR, seriya mathematicheskaya, 5, p. 85, 1941.

3. Selesnick, R. S., et al., A quiescent state of 3 to 8 MeV radiation belt electrons, Geophys. Res. Lett., 24, p. 1343, 1997.

4. Tysganenko, N. A., A model of the near magnetosphere with a dawn-dusk asymmetry—1. Mathematical structure, J. Geophys. Res. 107, A8, SMP-12, 2002.

5. Wiener, N., Extrapolation, interpolation, and smoothing of stationary time series, John Wiley, New York, 1949.